Submitted to the International Europhysics Conference on High Energy Physics HEP99,
Tampere, Finland, July 1999

Test of QCD Dynamics at Small Parton Momenta x at HERA

H1 Collaboration

Abstract

The production of high transverse momentum π°-mesons has been measured in deep-inelastic e-p scattering events at low Bjorken-x taken with the H1 detector at HERA. The measurement of single particles has been extended to the region of small angles w.r.t. the proton remnant (forward region in the laboratory reference frame) and down to very low values of $x \approx 5{\cdot}10^{-5}$. This region corresponds to central rapidity in the virtual photon-hadron system and is expected to be particularly sensitive to QCD evolution effects in final states. Differential cross-sections are presented of inclusive π°-meson production as a function of Bjorken-x and the four-momentum transfer Q^2 , and as a function of the transverse momentum and the pseudorapidity of the π°-mesons. A recent numerical BFKL calculation and predictions from QCD models based on DGLAP parton evolution are compared to the data.

Abstract: 157g
Parallel sessions: 1,3
Plenary sessions: 1,3

Electronic Access: http://www-h1.desy.de/publications/

1 Introduction

The hadronic final state in Deep-Inelastic Scattering (DIS) interactions at HERA, which collides 27.5 GeV positrons on 820 GeV protons, has been advocated [1, 2, 3, 4] over the last few years for its potential to provide new stringent tests on the physics of Quantum Chromodynamics (QCD), the theory of the strong interactions, in a kinematical region of high parton densities which so far has not been accessible. The high Center of Mass System (CMS) energy ($\sim$ 300 GeV) of the HERA collider allows a region in Bjorken-x of $\sim 10^{-5} - 10^{-4}$ to be reached, while keeping the momentum transfer, Q^2, larger than a few GeV^2, thus remaining in the regime of perturbative QCD (pQCD). In the DIS process a parton in the proton can induce a QCD cascade consisting of several subsequent parton emissions before the final parton interacts with the virtual photon. The multiplicity and the Bjorken-x distribution of these emitted partons differ significantly for different approximations of QCD dynamics at small x.

At low x QCD evolution is complicated by the occurrence of two large scales, namely $\ln 1/x$ and $\ln Q^2$, in contrast to the main testing region of pQCD so far at relatively large x, where a summation of the leading $\ln Q^2$ terms was sufficient. A complete perturbative treatment in the low-x region is not yet possible, so instead different approximations are made to the QCD evolution which predict widely different parton dynamics. These include QCD parton evolution schemes such as the classical DGLAP (Dokshitzer-Gribov-Lipatov-Altarelli-Parisi) [5] evolution equation, and the low-x specific BFKL (Balitsky-Fadin-Kuraev-Lipatov) [6] evolution equation. At high Q^2 pQCD requires the resummation of contributions of $\alpha_s \ln(Q^2/Q_0^2)$ terms, yielding the DGLAP evolution equations. However at small x the second large logarithm in $1/x$ may become important. Resummation of these terms leads to the BFKL evolution equation. Hence the pertinent and exciting question is whether these $\ln 1/x$ contributions to the parton evolution can be observed experimentally.

Differences between different dynamical assumptions on the parton cascade are expected to be emphasized in the region towards the proton remnant direction, i.e. away from the scattered quark. This region corresponds to central rapidity in the virtual photon-hadron system. In the HERA laboratory frame this corresponds to a region of small polar angles and has been generically termed "forward region"[1]. In previous analyses results have been presented on forward jet and forward single charged and neutral pion production [7, 8], based on data collected in 1994. A similar measurement has been presented by the ZEUS collaboration on forward jet production [9]. In this paper we study forward single π° production for a considerably larger data sample compared to [8] which was collected in 1996 and includes an enlarged kinematical range. The production of high p_T particles is strongly correlated to the emission of hard partons in QCD and is therefore sensitive to the dynamics of the strong interaction [10, 11, 12]. An advantage of studying single particles, as opposed to jets, is independence of any choice of jet finding algorithm and the potential to reach smaller angles than would be possible with jets with broad spatial extent. Single particle production is also expected to have a better correlation to partons than jets at lower parton transverse momenta. In this analysis π°'s are selected in DIS events at low x in the region of momentum transfer 2.0 $< Q^2 <$ 70.0 GeV^2. The π°'s are required to have a polar angle in the lab frame between 5° and 25°, and transverse momentum

[1]H1 uses a right-handed coordinate system with the z axis defined by the incident proton beam and the y axis pointing upward.

larger than 2.5 GeV in the hadronic CMS (contrary to the analysis in [8], where the transverse momentum cut-off of 1 GeV was in the laboratory frame). The hadronic CMS has the advantage of being more closely related to the hard subprocess. The increased transverse momentum cut as compared to the data presented in [8] enhances the sensitivity to hard parton emission in the QCD cascade and provides a hard scale for perturbative calculations. It also reduces significantly the sensitivity to soft hadronization effects.

Inclusive hard particle production can be directly obtained from perturbative calculations using the measured fragmentation functions. Such a calculation is available for the BFKL formalism [4] and will be compared to the data. In addition the measurements are compared to models using $\mathcal{O}(\alpha_s)$ QCD matrix elements and parton cascades according to the DGLAP evolution.

2 Experimental Apparatus

A detailed description of the H1 detector can be found elsewhere [13]. The following section briefly describes the components of the detector relevant to this analysis.

The hadronic energy flow and the scattered electron are measured with a liquid argon (LAr) calorimeter and a backward SPACAL calorimeter respectively. The LAr calorimeter [14] extends over the polar angle range $4^\circ < \theta < 154^\circ$ with full azimuthal coverage. It consists of an electromagnetic section with lead absorbers and a hadronic section with steel absorbers. With about $45\,000$ cells in total both sections are highly segmented in the transverse and the longitudinal direction, in particular in the forward region of the detector. The total depth of both sections varies between 4.5 and 8 interaction lengths in the region $4^\circ < \theta < 128^\circ$. Test beam measurements of the LAr calorimeter modules showed an energy resolution of $\sigma_E/E \approx 0.50/\sqrt{E\ [\mathrm{GeV}]} \oplus 0.02$ for charged pions and of $\sigma_E/E \approx 0.12/\sqrt{E\ [\mathrm{GeV}]} \oplus 0.01$ for electrons [14]. The hadronic energy measurement is performed by applying a weighting technique in order to account for the non-compensating nature of the calorimeter. The absolute scale of the hadronic energy is presently known to 4%. The scale uncertainty for electromagnetic energies is 3 % [15].

The SPACAL is a lead/scintillating fiber calorimeter which covers the region $153^\circ < \theta < 177.8^\circ$ with an electromagnetic section and a hadronic section. The energy resolution for the electromagnetic part is $7.5\,\%/\sqrt{E} \oplus 2.5\,\%$, the energy resolution for hadrons is $\sim 30\,\%/\sqrt{E}$ (E in GeV). The energy scale uncertainties are 1 $\%$ and 7 $\%$ for the electromagnetic section and hadronic section respectively. The timing resolution of better than 1 ns in both sections of the SPACAL is exploited to form a trigger decision and reject background.

The calorimeters are surrounded by a superconducting solenoid providing a uniform magnetic field of 1.15 T parallel to the beam axis in the tracking region. Charged particle tracks are measured in the central tracker (CT) covering the polar angular range $20^\circ < \theta < 160^\circ$ and the forward tracking (FT) system, covering the polar angular range $5^\circ < \theta < 25^\circ$. The CT consists of inner and outer cylindrical jet chambers, z-drift chambers and proportional chambers. The jet chambers, mounted concentrically around the beam line, provide up to 65 space points in the radial plane for tracks with sufficiently large transverse momentum.

A backward drift chamber (BDC) in front of the SPACAL with an angular acceptance of $151^\circ < \theta < 177.5^\circ$ serves to identify electron candidates and to precisely measure their direction. Using information from the BDC, the SPACAL and the reconstructed event vertex the polar angle of the scattered electron is known to about 0.7 mrad.

The luminosity is measured using the reaction $ep \to ep\gamma$ with two TlCl/TlBr crystal calorimeters, installed in the HERA tunnel. The electron tagger is located at $z = -33$ m and the photon tagger at $z = -103$ m from the interaction point in the direction of the outgoing electron beam.

3 Theoretical Predictions

Predictions for final state observables are available from Monte Carlo models using $\mathcal{O}(\alpha_s)$ matrix elements and parton cascades according to the DGLAP evolution, and from numerical calculations based upon the BFKL formalism. In the following we describe the models and calculations used.

3.1 Phenomenological QCD Models

Implementations of $\mathcal{O}(\alpha_s)$ matrix elements complemented by parton showers based on the DGLAP splitting functions are available in the programs LEPTO6.5 [16] and HERWIG5.9 [17]. The factorization and renormalization scales are set to Q^2. The predictions of these models should be valid in the DGLAP region of phase space: $\alpha_s(Q^2)\ln(Q^2/Q_0^2) \sim 1$ and $\alpha_s(Q^2)\ln(1/x) \ll 1$. In LEPTO the Lund string model as implemented in JETSET7.4 [18] is used to describe hadronization processes. HERWIG differs from LEPTO in that it also considers interference effects due to color coherence and uses the cluster fragmentation model for hadronization. The versions of LEPTO6.5 and HERWIG5.9 used consider only DIS processes in which the virtual photon is always point-like.

Recently a model has been proposed (RAPGAP2.06 [19]) which is also based on the DGLAP formalism but includes contributions from processes in which the virtual photon entering the scattering process can be resolved. The relative contribution from resolved processes depends on the scale at which the virtual photon is probed. As in [20] the factorization and renormalization scale in this paper is taken to be $Q^2 + p_T^2$ (p_T^2 of the partons from the hard subprocess). Direct photon-proton interactions, where the photon is considered point-like, are taken from LEPTO6.5.

The model calculations in this paper were made with the CTEQ4M [21] parton densities for the proton and the SAS-1D [22] parton densities for the virtual photon. QED Corrections are determined with the Monte Carlo program DJANGO6.2 [23].

In a previous paper [8] we have also compared the results with ARIADNE [24] and LDCMC [25]. ARIADNE4.08 provides an implementation of the Color Dipole Model (CDM) of a chain of independently radiating dipoles formed by emitted gluons [26]. Unlike LEPTO, the cascade of the CDM is not ordered in transverse momentum. For the present analysis it was confirmed that the predictions depend strongly on the parameters controlling the 'size' of the diquark and photon, and are therefore not explicitly compared with data in this paper[2]. The linked dipole chain (LDC) model [27] is a reformulation of the CCFM [28] equation, which forms a bridge between the BFKL and DGLAP approaches. Calculations of the hadronic final state based on this approach are available with the LDCMC 1.0 Monte Carlo which matches exact first order matrix elements with the LDC-prescribed initial and final state parton emissions. The model however failed to describe the data in [8] and is therefore not considered further in this paper.

3.2 BFKL Calculation in Order $\mathcal{O}(\alpha_s)$ and Fragmentation Functions

Recently in [4] predictions for π° cross-sections have been presented based on a modified BFKL evolution equation in order $\mathcal{O}(\alpha_s)$, and π° fragmentation functions. The modified evolution equations include the so called "consistency constraint" [29, 30] which limits the gluon emission at each vertex in the cascade to the kinematically allowed region. It is argued that this constraint embodies a major part of the the non-leading $\ln(1/x)$ contributions to the BFKL equation, which have been found to be very important [31]. The predictions of this modified BFKL equation are therefore expected to be more reliable than those without the constraint. The parton densities and fragmentation functions used in the calculation are taken from [32] and [33] respectively. In this paper we compare "set (iii)" of [4] to the data. In this set the scale for α_S is taken to be the transverse momentum of the emitted partons, k_T^2, and the infrared cut-off in the modified BFKL equation is taken to be 0.5 GeV^2. Calculations with these parameters give a fair description of the forward jet cross-sections from [8] when taking into account hadronization corrections. The predictions are labeled "mod LO BFKL" in the figures.

4 Measurement

4.1 Data Selection

The analysis is based on data representing an integrated luminosity of $\mathcal{L} = 5.8 \text{ pb}^{-1}$ taken by H1 during 1996. Deep-inelastic scattering events are selected and the event kinematics are calculated from the polar angle and the energy of the scattered positron. The negative square of the four momentum transfer, Q^2 , and the inelasticity y are related to these quantities (neglecting the positron mass) by: $Q^2 = 4\,E_e\,E_l \cos^2\frac{\theta_e}{2}$ and $y = 1 - \frac{E_e}{E_l}\sin^2\frac{\theta_e}{2}$, where E_l and E_e are the energies of the incoming and the scattered positron respectively and θ_e is the polar angle of the scattered positron. Bjorken-x is then given by $x = Q^2 / (y \cdot s)$, where s is the square of the center of mass energy. Experimentally the scattered positron is defined to be the highest energy cluster, i.e. localized energy deposit, in the SPACAL with a cluster radius of

[2]A good description of the data presented in this paper can be achieved (now with ARIADNE4.10) e.g. choosing PARA(10)=1.7 and PARA(14)=1.0 [12].

less than 3.5 cm and an associated track in the BDC. Experimental requirements based on the energy and the polar angle of the scattered positron are used during the preselection but these are superseded by stronger kinematic cuts which restrict the data to the range $0.1 < y < 0.6$ and $2.0 < Q^2 < 70.0$ GeV^2. Photoproduction background is reduced to a negligible level by requiring $35 < \sum_j (E_j - p_{z,j}) < 70$ GeV [34] with E_j and $p_{z,j}$ the energy and longitudinal momentum of a particle respectively, and where the sum extends over all detected particles in the event. The reconstruction of the primary event vertex must yield a z coordinate not more than 35 cm away from the nominal interaction point. The trigger is based on energy depositions in the SPACAL and track activity in the central tracker. For the events used in this analysis the efficiency of this trigger is around 80 $\%$, determined using information from monitor trigger data. After the selection about 600k events are available for further analysis.

4.2 Forward π°-Meson Selection

A measurement of parton emission at mid rapidity in the hadronic CMS system requires small forward angles in the lab system. This area is not well instrumented to measure charged particle cross-sections. The finely segmented H1 calorimeter however allows the measurement of π°'s down to very small angles. They are measured using the dominant decay channel $\pi^\circ \to 2\gamma$. The π° candidates are selected in the region $5^\circ < \theta_\pi < 25^\circ$, where θ_π is the polar angle of the produced π°. Candidates are required to have an energy of $x_\pi = E_\pi / E_{proton} > 0.01$, with E_{proton} the proton beam energy (820 GeV), and a transverse momentum in the hadronic CMS, $p^\star_{T,\pi}$, greater than 2.5 GeV. At the high π° energies considered here, the two photons from the decay cannot be separated, but appear as one object (cluster) in the calorimetric response. Therefore, the standard method of reconstructing the invariant mass from the separate measurement of the two decay photons to identify the π°-meson is not applicable.

Instead, a detailed analysis of the longitudinal and transverse shape of the energy depositions is performed to separate electromagnetic and hadronic showers. This approach is based on the compact nature of electromagnetic showers as opposed to showers of hadronic origin, which are broader. The analysis of shower forms is made possible by the fine granularity of the H1 LAr calorimeter in the forward direction which has a cell size of 3.5×3.5 cm^2 (comparable to the mean Moliere radius $\bar{R}_m = 3.6$ cm and the mean radiation length $\bar{X}_0 = 1.6$ cm) and four-fold longitudinal segmentation for the electromagnetic section which has a thickness of 20 to 25 X_0. The main experimental challenge in this analysis is the high activity in this region of phase space, with hadronic showers “masking” the clear electromagnetic signature provided by the two photons of a π° decay. The overlap of a π° induced cluster with another hadron is mainly responsible for losses of π° detection efficiency, since the distortion of the shape estimators it causes will, in many cases, lead to the rejection of the cluster candidate.

The reconstruction of LAr data is optimized to contain all energy of an electromagnetic shower into one cluster. A π°-meson candidate is required to be a cluster with more than 90 $\%$ of its energy deposited in the electromagnetic part of the LAr calorimeter. A “hot” core consisting of the most energetic group of continuous electromagnetic calorimeter cells of a cluster, which must include the hottest cell, is defined for each candidate [35]. More than 50 $\%$ of the cluster energy is required to be deposited in this core. The lateral spread of the shower is quantified in terms of lateral shower moments calculated relative to the shower's principal axis [35] and required to be less than 4 cm [12]. The longitudinal shower shape is used as a selection criterion via the fraction of the shower's energy deposited in each layer of cells in the electromagnetic part of the calorimeter. The precise specifications of these layers can be found in [35]. The value of the part of the cluster's energy measured in the second layer minus that part measured in the fourth layer is required to be more than 0.4 times the total cluster energy, thereby selecting showers which start to develop close to the calorimeter surface and are well contained in the electromagnetic part of the calorimeter, as expected for showers of electromagnetic origin. As mentioned above with this selection one can not distinguish photons from a π°-meson decay and photons from other sources. The high energy required in the selection however ensures that contributions from sources other than high energy π°-mesons (such as prompt photon production) are at a negligible level [36].

With this selection about 1700 (600) π° candidates are found in the kinematic range $5^\circ < \theta_\pi < 25^\circ$, $x_\pi > 0.01$ and $p^\star_{T,\pi} >$ 2.5 (3.5) GeV with a detection efficiency better than 45 $\%$.

Monte Carlo studies using a detailed simulation of the H1 detector for a sample of DIS events, yield a purity of about 70 % for the selected π°-meson sample, with impurities from misidentified hadrons and from secondary interactions of charged hadrons with passive material in the detector. These studies show that less than 10 $\%$ of the selected π° candidates stem from secondary scattering of charged hadrons with passive material in the forward region, where the amount of material between the interaction point and the calorimeter surface is largest.

The determination of π° acceptance and purity depends only on the particle density and energies in the forward calorimeter. To ensure that the different MC models used are in reasonable agreement with the data in this respect the transverse energy flow around the π° candidate clusters was studied in detail. Both the E_T flow and the E_T spectra in the tail of the E_T flow distributions are reasonably well described by the models used to estimate the detector corrections [12]. Of the two models used, however, ARIADNE showed a higher particle density while LEPTO has a lower particle density than the data. Remaining differences of the correction functions determined with the two MC's are therefore used to estimate the systematic error. When the energy and transverse momentum requirements are lowered the two photons from the π° decay become separable and a clear π° mass peak can be observed which is also well reproduced by the H1 detector simulation. The same method of selecting π°-mesons was used in a previous H1 analysis [8], where a measurement of charged particle tracks in the same region was also performed. The measured π° data and the cross-sections of $(\pi^+ + \pi^-)/2$ obtained from the charged particle measurements were found to agree well. Furthermore, the results of the analysis of the 1994 data are found to be in good agreement with the present analysis in their region of common phase space.

5 Results

The experimental results of the analysis are presented as differential cross-sections of forward π°-meson production as a function of Q^2 , and as a function of x, η_π and $p^\star_{T,\pi}$ in three regions of Q^2 for $p^\star_{T,\pi} > 2.5$ GeV. The pseudorapidity η_π is given by $-\ln\left[\tan\left(\theta/2\right)\right]$ with θ being the polar angle of the π° in the laboratory frame. In addition the π° cross-sections as a function of x and Q^2 are measured for data with the lower threshold of the π° transverse momentum increased to $p^{\star}_{T,\pi} > 3.5$ GeV. The phase space is given by $0.1 < y < 0.6$, $2.0 < Q^2 < 70.0$ GeV^2, $5^\circ < \theta_\pi < 25^\circ$ and $x_\pi = E_\pi / E_{proton} > 0.01$ in addition to the $p^{\star}_{T,\pi}$ thresholds given above. θ_π and x_π are taken in the H1 laboratory frame; $p^{\star}_{T,\pi}$ is calculated in the hadronic CMS. The measurement extends down to $x = 5{\cdot}10^{-5}$, covering two orders of magnitude in x.

All observables are corrected for detector effects and for the influence of QED radiation by a bin-by-bin unfolding procedure. The detector effects include the efficiency, purity and acceptance of the π°-meson identification as well as contributions from secondary scattering in passive material. The correction functions are obtained with two different models (ARIADNE and LEPTO). The final correction is performed with the average of the two models. The spread of the two models is taken as an estimate of the systematic uncertainty associated with the model dependence of the correction.

The typical total systematic uncertainty is 15-25 $\%$, compared to a statistical uncertainty of about 10 $\%$. Contributions to the systematic error include: the uncertainty of the luminosity measurement (less than 2 $\%$), the statistical uncertainty in the determination of the trigger efficiency (5 $\%$), the uncertainty of the electromagnetic energy scale of the LAr (3%) and the SPACAL (1%) calorimeter which each contribute 5-10 $\%$, the variation of π°-meson selection and acceptance requirements by their respective resolutions (5-10 $\%$), and the model dependence of the bin-by-bin correction procedure, by using differences found from ARIADNE and LEPTO (5-10 $\%$). The remaining background from photoproduction has been studied using a sample of photoproduction Monte Carlo events (PHOJET [37]) representing an integrated luminosity of about 1 pb^{-1}. The contribution from such events is found to be negligible in all bins.

The cross-sections as a function of x shown in Figure 1(a) exhibit a strong rise towards small x. An interesting observation however is that this rise in x is identical to the rise of the total inclusive cross-section as measured e.g. in [38] as demonstrated in Fig. 1(b). It shows the rate of π°-meson production in DIS as a function of x obtained by dividing the cross-section shown in Fig. 1(a) by the inclusive ep cross-section in each bin of x, y and Q^2 . The total cross-section is obtained by integrating the H1 QCD fit to the 1996 structure function data as presented in [38] for every bin of the present measurement of inclusive π°-meson cross-sections. Note however that the π° rate increases with increasing Q^2. The shapes of $d\sigma_\pi/d\eta_\pi$ and $d\sigma_\pi/dp^{\star}_{T,\pi}$ (Fig. 2) show no significant dependence on the regions of Q^2 in which they are measured. Figure 3 shows the inclusive π°-meson cross-section as a function of Q^2 . The cross-section falls steeply with increasing Q^2. Figure 4 finally shows $d\sigma_\pi/dQ^2$ and $d\sigma_\pi/dx$ for the higher threshold of $p^{\star}_{T,\pi} > 3.5$ GeV. No significant change in shape of the distributions occurs when the $p^{\star}_{T,\pi}$ threshold is raised, but the cross-sections are reduced by about a factor of three.

All differential cross-sections are compared to three predictions based on different QCD approximations. The DGLAP prediction for the pointlike virtual photon scattering (including parton showers) as given by LEPTO6.5 falls clearly below the data. There is still a fair agreement with data for the highest x and Q^2 bins, shown in Fig. 1(a) and Fig. 3, but differences between the prediction and data occur in the low-x region. These differences are as large as a factor of five in the lowest x region. The mechanism of emitting partons according to the DGLAP splitting functions, combined with pointlike virtual photon scattering only, is clearly not supported by the data, in particular at low x. The LEPTO prediction is based on about seven times the integrated luminosity of the data. Comparisons to HERWIG5.9 [17] lead to similar conclusions [12].

A considerable improvement of the description of the data is achieved by a model which considers in addition processes where the virtual photon entering the scattering process is resolved. This can be regarded as an approach to make an effective resummation of higher order corrections. It also provides a smooth transition towards the limit of $Q^2 = 0$. i.e. photoproduction where resolved processes dominate in the HERA regime. Such a prediction is provided by RAPGAP2.06 [19]. In Fig. 1(a) RAPGAP2.06 can be seen to predict cross-sections very close to the measured distributions with the exception of the lowest Q^2 bin where the prediction is too low. All predicted cross-sections increase by up to 30 $\%$ when the scale in the hard scattering is increased from $Q^2 + p_T^2$ to $Q^2 + 4p_T^2$ [12], and hence does not improve the overall description. Whether this mechanism is adequate to describe the π° cross-sections down to the lowest available x cannot therefore be conclusively demonstrated by RAPGAP2.06. The RAPGAP prediction is based on approximately four times the integrated luminosity of the data.

Next we compare the data with a prediction of the semi-inclusive cross-section based on a modified LO BFKL parton calculation convoluted with π° fragmentation functions. The predictions obtained with these calculations turn out to be in good agreement with the neutral pion cross-sections measured in the entire available phase space with a slight tendency to be below the data at the lowest values of Q^2. Figure 2(a) indicates that the existing discrepancies occur mostly at the largest accessible values of η_π. The predictions involve a cut-off parameter in the transverse momentum k_t^2 of the partons: k_0^2=0.5 GeV^2 and a choice of renormalization scale. It is shown in [4] however that a variation of k_0^2 by a factor of two leads to less than a 10% change of the prediction. The scale dependence is larger; a change from k_T^2 to $k_T^2/4$ leads to an approximate increase of 60% in the predictions. This affects mostly the normalization, and not the shape of the predictions. The good agreement between this prediction and the data suggests that the modified BFKL evolution equation, using the consistency constraints, is a good approximation for low-x evolution in the considered phase space.

The shapes of the η_π and $p_{T,\pi}^\star$ spectra shown in Fig. 2 are well described by all models. The conclusions on the comparison of the model predictions with the data are the same for the higher $p_{T,\pi}^\star$ cut-off of the data, as shown in Fig. 4.

6 Conclusions

Differential cross-sections of forward π° production have been measured for particles with $p_{T,\pi}^\star >$ 2.5 (3.5) GeV, $5^\circ < \theta_\pi < 25^\circ$ and $x_\pi = E_\pi / E_{proton} >$ 0.01, for DIS events in the region $0.1 < y <$ 0.6 and 2.0 $< Q^2 <$ 70.0 GeV^2. The data provide a measurement of QCD parton dynamics at low x (high parton density) and mid-rapidity in the hadronic CMS system. They are found to be discriminative towards different approximations to QCD evolution in this kinematic regime. The data therefore provide an important testing ground for QCD in the new regime opened up by HERA.

Models using $\mathcal{O}(\alpha_s)$ QCD matrix elements and parton cascades according to the DGLAP splitting functions cannot describe the differential neutral pion cross-sections at low x. The inclusion of processes in which the virtual photon is resolved leads to an improved description of the data. Renormalization and factorization scale uncertainties however limit the precision of the predictions. A calculation based on the BFKL formalism is in good agreement with the data, particularly for the shape, but the absolute normalization remains strongly affected by the scale uncertainty. So far the data in the phase space selected in this analysis could not be confronted with a NLO prediction – either for DGLAP or for BFKL. More definite conclusions therefore have to be delayed until these NLO calculation can be confronted with the data.

Acknowledgments

We wish to thank A.D. Martin and J.J. Outhwaite for useful discussions. We are grateful to the HERA machine group whose outstanding efforts have made and continue to make this experiment possible. We thank the engineers and technicians for their work constructing and maintaining the H1 detector, our funding agencies for financial support, the DESY technical staff for continual assistance and the DESY directorate for the hospitality which they extend to the non-DESY members of the collaboration.

References

[1] A.H. Mueller, Nucl. Phys. B (Proc. Suppl.) **18C** (1990) 125;
J. Phys. **G17** (1991) 1443.

[2] J. Kwieciński, A.D. Martin, P.J. Sutton, Phys. Rev. **D46** (1992) 921.

[3] J. Bartels, A. De Roeck, M. Loewe, Z. Phys. **C54** (1992) 635;
W.K. Tang, Phys. Lett. **B278** (1992) 363.

[4] J. Kwiecinski, A.D. Martin, J.J. Outhwaite, hep-ph/9903439, to be published in Eur. Phys. J. **C**.

[5] V.N. Gribov and L.N. Lipatov, Sov. J. Nucl. Phys. **15** (1972) 438 and 675;
Yu. L. Dokshitzer, Sov. Phys. JETP **46** (1977) 641;
G. Altarelli and G. Parisi, Nucl. Phys. **126** (1977) 297.

[6] E.A. Kuraev, L.N. Lipatov and V.S. Fadin, Sov. Phys. JETP **45** (1972) 199; Y.Y. Balitsky and L.N. Lipatov, Sov. J. Nucl. Phys. **28** (1978) 822.

[7] H1 Collab., S. Aid et al., Phys. Lett. **B356** (1995) 118.

[8] H1 Collab., C. Adloff et al., Nucl. Phys. **B538** (1999) 3.

[9] ZEUS Collab., J. Breitweg et al., Eur. Phys. J. **C6** (1999) 239.

[10] M. Kuhlen, Phys. Lett. **B382** (1996) 441.

[11] H1 Collab., C. Adloff et al., Nucl. Phys. **B485** (1997) 3.

[12] T. Wengler, PhD thesis, University of Heidelberg, January 1999, DESY-THESIS-1999-011.

[13] H1 Collab., I. Abt et al., Nucl. Instr. and Meth. **A386** (1997) 310 and Nucl. Instr. and Meth. **A386** (1997) 348.

[14] H1 Calorimeter Group, B. Andrieu et al., Nucl. Instr. and Meth. **A336** (1993) 460 and 499.

[15] H1. Collab., Measurement of the Neutral and Charged Current Cross-Sections in Positron-Proton Collisions at Large Momentum Transfer, in preparation.

[16] G. Ingelman, A. Edin and J. Rathsman, Comp. Phys. Comm. **101** (1997) 108.

[17] G. Marchesini et al., Comp. Phys. Comm. **67** (1992) 465;
M.H. Seymour, Nucl. Phys. **B436** (1995) 443.

[18] T. Sjöstrand, Comp. Phys. Comm. **39** (1986) 347;
T. Sjöstrand and M. Bengtsson, ibid. **43** (1987) 367.

[19] H. Jung, Comp. Phys. Comm. **86** (1995) 147;
(for update see http://www-h1.desy.de/~jung/rapgap/rapgap.html).

[20] H. Jung, L. Jönsson and H. Kuester, DESY 98-051, hep-ph/9805396.

[21] CTEQ Collab., H.L. Lai et al., Phys.Rev. **D55** (1997) 1280.

[22] G.A. Schuler, T. Sjostrand, Phys. Lett. **B376** (1996) 193.

[23] K. Charchula, G. Schuler, H. Spiesberger, Comp. Phys. Comm. **81** (1994) 381.

[24] L. Lönnblad, Comp. Phys. Comm. **71** (1992) 15.

[25] H. Kharraziha and L. Lönnblad, hep-ph/9709424.

[26] G. Gustafson and Ulf Petterson, Nucl. Phys. **B306** (1988);
G. Gustafson, Phys. Lett. **B175** (1986) 453;
B. Andersson, G. Gustafson, L. Lönnblad, Ulf Petterson, Z. Phys. **C43** (1989) 625.

[27] B. Andersson, G. Gustafson, J. Samuelsson, Nucl. Phys. **B467** (1996) 443;
B. Andersson, G. Gustafson, H. Kharraziha, J. Samuelsson, Z. Phys. **C71** (1996) 613.

[28] M. Ciafaloni, Nucl. Phys. **B296** (1988) 49;
S. Catani, F. Fiorani and G. Marchesini, Phys. Let. **234B** (1990) 339 and
Nucl. Phys. **B336** (1990) 18.

[29] J. Kwiecinski, A.D. Martin and P.J. Sutton, Z. Phys. **C71** (1996) 585.

[30] J. Kwiecinski, A.D. Martin and A.M. Stasto, Phys. Rev. **D56** (1997) 3991.

[31] V.S. Fadin and L.N. Lipatov, Phys. Lett. **B429** (1998) 127.

[32] A.D. Martin, R.G. Roberts, W.J. Stirling, R.S. Thorne, Eur. Phys. J. **C4** (1998) 463.

[33] J. Binnewies, B.A. Kniehl and G. Kramer, Phys.Rev. **D52** (1995) 4947.

[34] H1 Collab., S. Aid et al., Nucl. Phys. **B470** (1996) 3.

[35] H1 Calorimeter Group, B. Andrieu, et al., Nucl. Instr. and Meth. **A334** (1994) 492.

[36] J. Kwiecinski, S.C. Lang and A.D. Martin, Phys. Rev. **D55** (1997) 1273;
hep-ph/9707240.

[37] R. Engel, Z. Phys. **C66** (1995) 203;
R. Engel and J. Ranft, Phys. Rev. **D54** (1996) 4244.

[38] H1 Collab., C. Adloff et al., Contributed paper (260) to HEP97 Jerusalem, August 9-26, 1997.

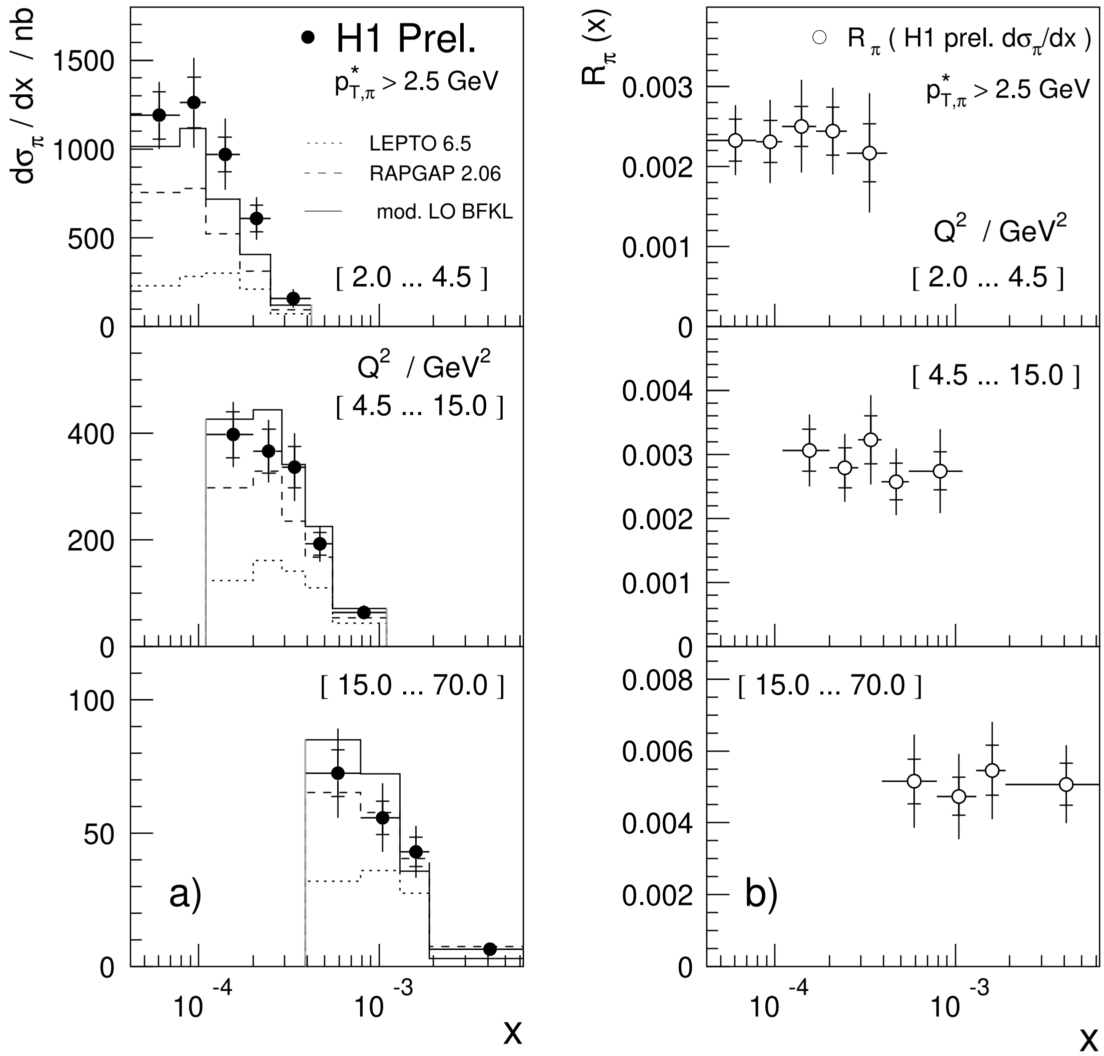

Figure 1: Inclusive π°-meson production cross-sections as a function of x for $p^\star_{T,\pi} > 2.5$ GeV in three regions of Q^2 (a). The phase space is given by $0.1 < y < 0.6$, $5^\circ < \theta_\pi < 25^\circ$ and $x_\pi = E_\pi/E_{proton} > 0.01$ in addition to the restrictions given in the figure. θ_π and x_π are measured in the H1 laboratory frame, $p^\star_{T,\pi}$ is calculated in the hadronic CMS. The two QCD models RAPGAP (direct and resolved contributions) and LEPTO are compared to the data. Also shown is the prediction of the modified LO BFKL calculation by Kwiecinski, Martin and Outhwaite. Figure (b) shows the rate of π°-meson production in DIS as a function of x obtained by dividing the cross-section shown in Figure (a) by the inclusive ep cross-section in each bin of x, y and Q^2 .

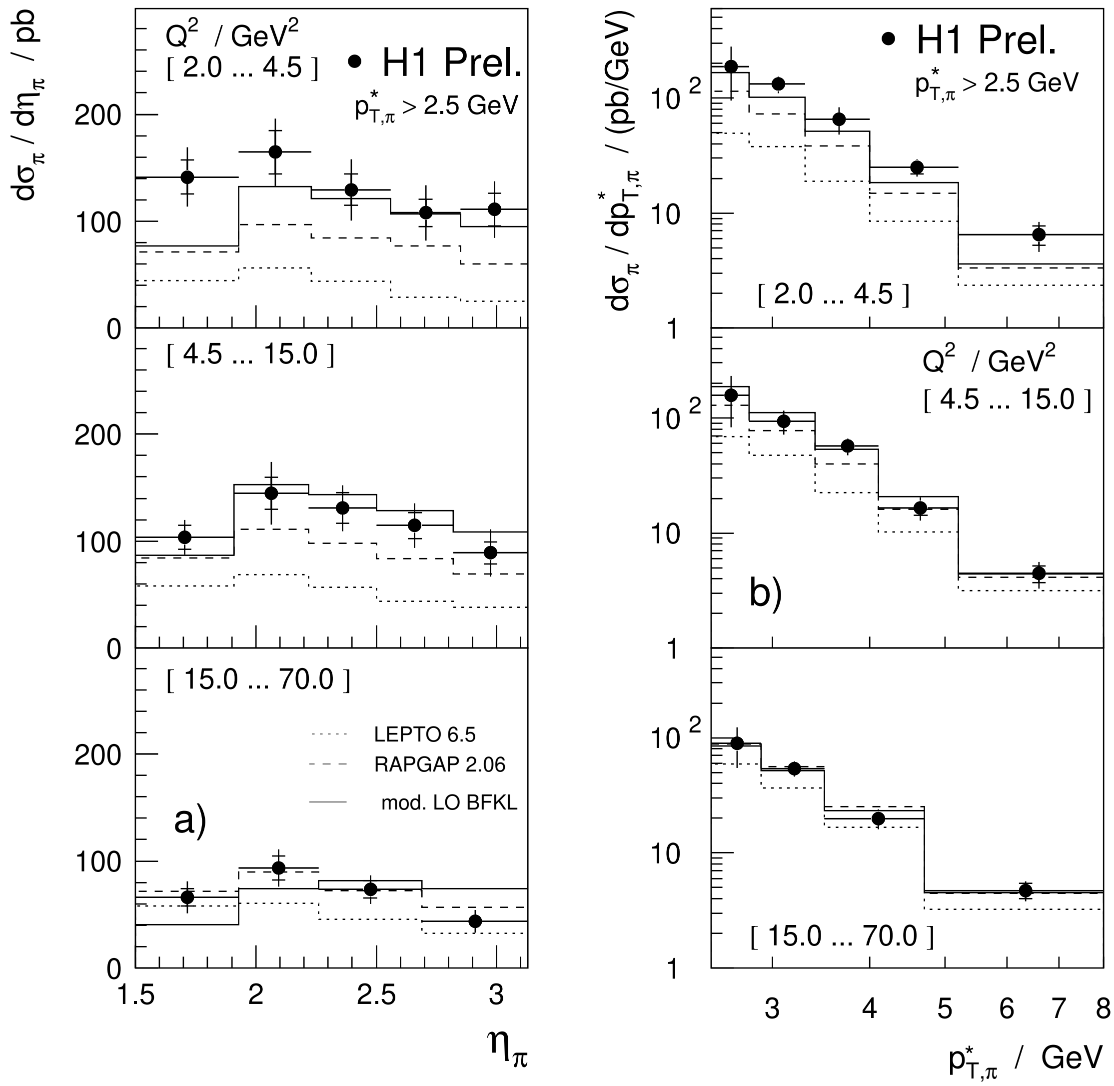

Figure 2: Inclusive π°-meson production cross-sections as a function of η_π (a) and $p^{\star}_{T,\pi}$ (b) for $p^{\star}_{T,\pi} > 2.5$ GeV in three regions of Q^2 . The phase space is given by 0.1 $< y <$ 0.6, $5^\circ < \theta_\pi < 25^\circ$ and $x_\pi = E_\pi / E_{proton} >$ 0.01 in addition to the restrictions given in the figure. θ_π and x_π are measured in the H1 laboratory frame, $p^{\star}_{T,\pi}$ is calculated in the hadronic CMS. The two QCD models RAPGAP (direct and resolved contributions) and LEPTO are compared to the data. Also shown is the prediction of the modified LO BFKL calculation by Kwiecinski, Martin and Outhwaite.

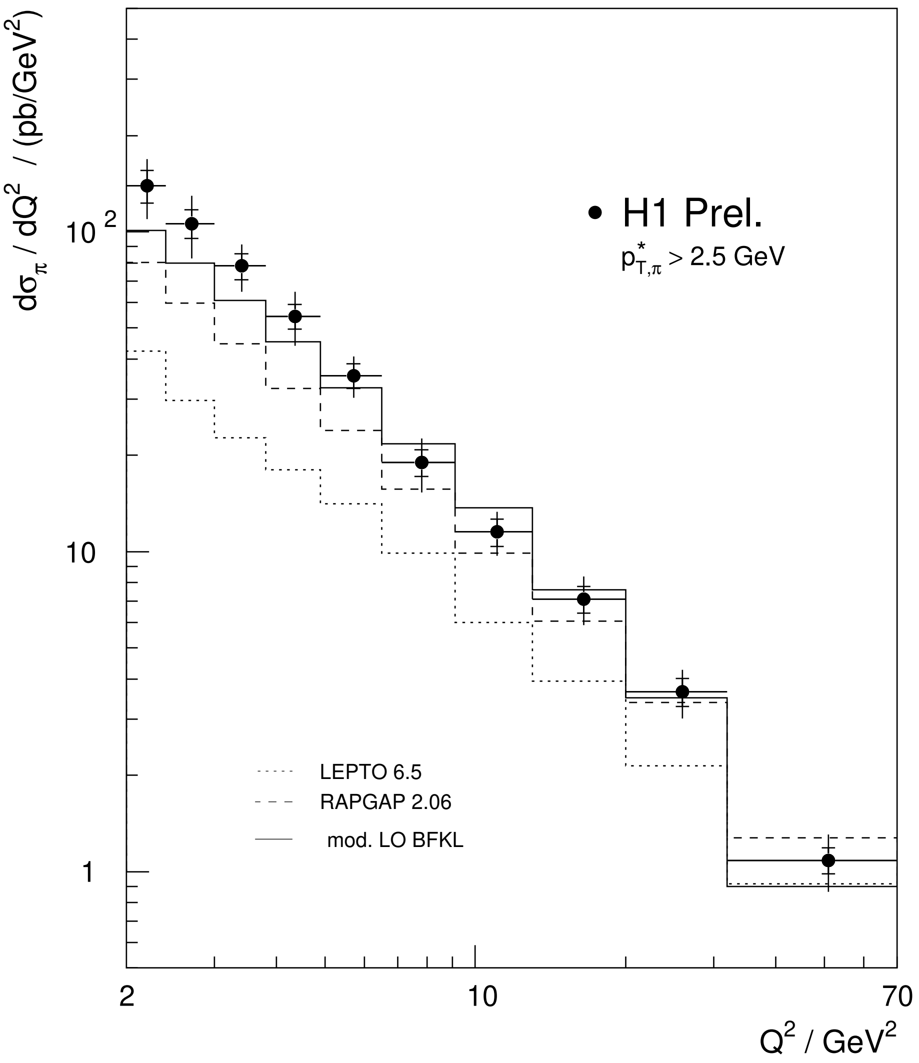

Figure 3: Inclusive π°-meson production cross-sections as a function of Q^2 for $p^\star_{T,\pi} > 2.5$ GeV. The phase space is given by $0.1 < y < 0.6$, $5^\circ < \theta_\pi < 25^\circ$ and $x_\pi = E_\pi / E_{proton} > 0.01$. θ_π and x_π are measured in the H1 laboratory frame, $p^\star_{T,\pi}$ is calculated in the hadronic CMS. The two QCD models RAPGAP (direct and resolved contribution) and LEPTO are compared to the data. Also shown is the prediction of the modified LO BFKL calculation by Kwiecinski, Martin and Outhwaite.

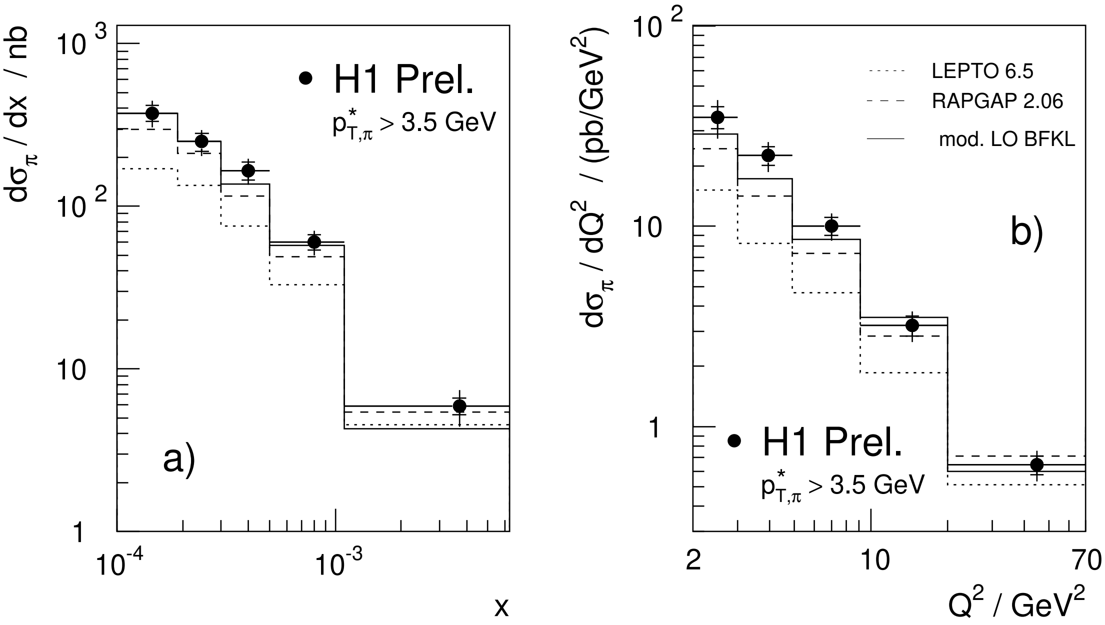

Figure 4: Inclusive π°-meson production cross-sections as a function of x (a) and Q^2 (b) for $p^\star_{T,\pi} > 3.5$ GeV. The phase space is given by 2.0 < Q^2 < 70.0 GeV^2 , 0.1 < y < 0.6, $5^\circ <$ $\theta_\pi < 25^\circ$ and $x_\pi = E_\pi/E_{proton} >$ 0.01. θ_π and x_π are measured in the H1 laboratory frame, $p^\star_{T,\pi}$ is calculated in the hadronic CMS. The two QCD models RAPGAP (direct and resolved contribution) and LEPTO are compared to the data. Also shown is the prediction of the LO BFKL calculation by Kwiecinski, Martin and Outhwaite.